

# Reinforcing Thermosets with Crystallizable Solvents

ONUR SINAN YORDEM, ALAN J. LESSER

Polymer Science and Engineering Department, University of Massachusetts, Amherst, Massachusetts 01003

Received 21 October 2009; revised 1 December 2009; accepted 7 January 2010

DOI: 10.1002/polb.21955

Published online in Wiley InterScience (www.interscience.wiley.com).

**ABSTRACT:** This study demonstrates an approach to generate reinforcement in thermosetting polymers through crystal growth of crystallizable solvents. Emphasis is to identify the reaction conditions, which lead to suitable reinforcement in selected compounds. Crystallization behavior and miscibility of dimethylsulfone (DMS) in diglycidylether of bisphenol-A epoxy monomer was investigated. Small angle laser scattering and optical microscopy were utilized to monitor phase separation and crystallization of DMS at different isothermal conditions during the cure process. It is shown that DMS crystals grow anisotropically to form faceted geometries and demonstrate possible structures to anchor into the epoxy matrix. The

growth mechanism and the agility of crystals are shown to be affected by the cure reaction as well as depth of supercooling. A completely cured sample with 15 wt % DMS shows a broad map of rich morphologies from nanoscale particles to uniformly distributed macroscale, discontinuous fiber-like crystals generated only by altering the curing conditions. © 2010 Wiley Periodicals, Inc. *J Polym Sci Part B: Polym Phys* 48: 840–849, 2010

**KEYWORDS:** composites; crystallization; *in situ* reinforced thermoset; nanocrystal; phase separation

**INTRODUCTION** Thermoset matrix composites make up an expansive and important class of engineering materials that are used in a variety of communities. Discontinuous or “chopped” fiber-reinforced polymer matrix composites are commonplace in many applications today ranging from marine, to automotive, to sporting goods. This class of materials is attractive as the discrete fibers impart increased stiffness and strength obtained beyond that which the polymer matrix can provide. However, this approach to reinforce polymers has many major drawbacks including processing limits as the viscosity increases tremendously by the addition of the rigid reinforcement.<sup>1,2</sup> Processing this class of materials also can have detrimental effects on the final composite performance as the fibers themselves can fracture during extrusion or molding.<sup>3–5</sup>

*In situ*-based liquid crystalline (LC) thermosets have seen a vast amount of interest in the last few decades. The chemistry to form a LC crosslinked network requires specific epoxy monomers to impart the LC phase;<sup>6–8</sup> therefore, the reinforcing options are limited due to selective chemistry. Development of anisotropic reinforcement in LC composites requires an application of external field during curing. LC domains have little aspect ratio when cured in quiescent conditions. The fact that a force field is needed to generate anisotropy indicates a practical limitation to mass production and imparts nonuniform orientation with increased thickness of the sample.<sup>7</sup> The generated LC phase is fixed in the network during the cure reaction; thus, the level of anisotropy

depends on the thermal cure conditions<sup>6</sup> and applied force fields, and only fibrillar morphologies can be obtained within the LC phase.

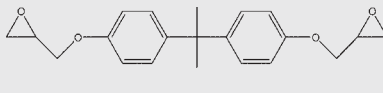
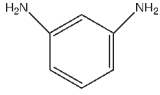
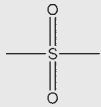
This article presents initial results of a larger study to investigate the potential of using crystallizable solvents as a means to provide self-reinforcement in thermosets. The approach involves introducing a low molecular weight (LMW) organic additive that melts and becomes miscible with the resin before polymerization. At this early stage the resin has a lower viscosity than that of the unmodified resin; thereby enhancing its processibility.<sup>9</sup> As the resin is allowed to polymerize, the additive undergoes phase separation followed by or concomitant with crystallization to produce crystals embedded within the polymer. A similar study by our group was reported by Yoon et al., where they concentrated on reinforcing polypropylene and polyethylene with crystallizable solvents and additives, such as pyrene and tetrabromobisphenol-A.<sup>10</sup> Both of these approaches are also part of a recent patent on this technology.<sup>11</sup> In another related work, LMW solvents were dispersed in thermosets;<sup>12</sup> however, the potential morphologies due to the crystallization of the LMW solvent was not investigated.

In the case reported herein, LMW organic compounds, under certain conditions, phase separate in the matrix and form crystals with a variety of rich morphologies. It is known that LMW organic compounds form needle-like, dendritic, and small sphere-like but faceted crystals.<sup>13</sup> By selecting a LMW compound with a crystallization temperature in the vicinity

Correspondence to: A. J. Lesser (E-mail: ajl@polysci.umass.edu)

*Journal of Polymer Science: Part B: Polymer Physics*, Vol. 48, 840–849 (2010) © 2010 Wiley Periodicals, Inc.

**TABLE I** List of Materials and Their Chemical Structures

Chemical Name	Structure
DGEBA	
1,3-Phenylenediamine	
Dimethylsulfone	

of the curing temperature of the epoxy, competition between phase separation and isothermal crystallization can be achieved. This competition leads to formation of composites containing a broad range of reinforcement morphologies. Herein, emphasis is given on the morphologies obtained by allowing dimethylsulfone (DMS) undergo phase separation and subsequent crystallization inside a curing epoxy.

## EXPERIMENTAL

### Materials

All materials were purchased from Aldrich Chemical unless otherwise noted and used without further purification. Epon<sup>TM</sup> 828, a diglycidylether of bisphenol-A (DGEBA) resin, supplied by Resource Resins, was used as the epoxide monomer. The aromatic resins were formulated using 1,3-phenylenediamine (mPDA) crosslinking agent. The LMW compound DMS is used as the organic crystal in the glassy network. The structures of the chemicals are provided in Table 1.

### Sample Preparation

In the first part of this study, the crystallization, the solubility, and the miscibility limit of DMS in DGEBA resin is investigated by using TA instruments Q200 differential scanning calorimeter (DSC). Samples were prepared in two steps. First, DMS and DGEBA were melt-blended at 120 °C in glass vials until a homogeneous solution was formed. Later, the vials were quenched in liquid nitrogen for 5 min. Blends of 5, 10, 15, 20, and 25 wt % DMS were prepared. It is important to point out that the crosslinking agent (mPDA) was not added to any of the samples for the miscibility experiments.

Additional studies focused on the phase separation and crystallization of DMS during the cure reaction of epoxy. These studies involved the use of a home-made small angle laser scattering (SALS) set-up, DSC, and optical microscopy. Samples were prepared in three steps. DGEBA resin and DMS were melt-blended at 120 °C in glass vials. Following a homogeneous solution formation, crosslinking agent (mPDA) was added at this temperature under continuous vigorous stirring for 30 s. Finally, the solution was quenched in liquid nitrogen for 5 min to minimize the curing reaction. Blends of

5, 10, 15, 20, and 25 wt % DMS were prepared. All of the samples were kept at −10 °C before analysis and used in 2 days period at most. Larger specimens were produced in glass vials and glass plaques following the same procedure given here.

### Characterization

DSC was conducted with a TA Instruments Q200 and used to monitor the change in crystallization behavior of DMS in the DGEBA medium as well as the miscibility limit of the solution. After the specimens were prepared, following the previously given procedure, 5–10 mg of sample was collected from the quenched mixture and put into an aluminum hermetic DSC pan. Two heating and cooling cycles were applied to the samples in the temperature range −50 to +130 °C with a constant rate of 10 °C/min unless otherwise noted. The instrument was calibrated using sapphire disks and keeping the helium flow rate constant at 25 μL/min. The first heating ramps show effects of thermal histories as a consequence of initial preparation of the DGEBA-DMS blends. Therefore, the miscibility and crystallization characterizations are performed on the cooling and the second heating ramps after erasing the thermal history.

The SALS setup used in this investigation is comprised of a linear polarized laser (Uniphase 1125P, HeNe λ: 632.8 nm); a polarizer set parallel to the laser polarization, a Linkam TMS93 heating stage where the sample is placed, and an image screen to collect scattered image. The image is captured from the projected scattering beams using a CCD Camera (Panasonic CCTV camera WVBP330). The scattered light intensity is measured by a photodiode. A home-made Lab VIEW protocol was used to collect all information simultaneously. Polymerization reaction of DGEBA resin and mPDA at isothermal conditions: 50, 60, 70, 80, and 90 °C were conducted simultaneously with crystallization of DMS. An illustration of the SALS setup is given in Figure 1. The samples were collected from quenched mixtures of DGEBA, DMS, and mPDA that were prepared following the previously given recipe in the Experimental Section. A small amount of mixture was placed between two clean glass slides, which were then placed into a heating stage. As the sample was heated and cooled, data from scattered image, intensity, temperature, and time were captured every 10–30 s in accordance with the rate of crystallization of DMS.

Optical Microscopy was conducted with Olympus BX51 and used to analyze samples after SALS experiments to examine the size and morphologies of the DMS crystals.

## RESULTS AND DISCUSSION

### Anticipated Phase Behavior

A Flory–Huggins (FH) lattice treatment<sup>14</sup> was initially used to estimate the phase behavior. Gibbs free energy of mixing formula was derived by Flory and Gibbs for linear polymer and solvent mixtures, however, it may be applicable to thermoset polymers when certain assumptions are considered.<sup>15–18</sup> Following Mezzenga et al.'s approach, the free energy of mixing equation is written in terms of volume

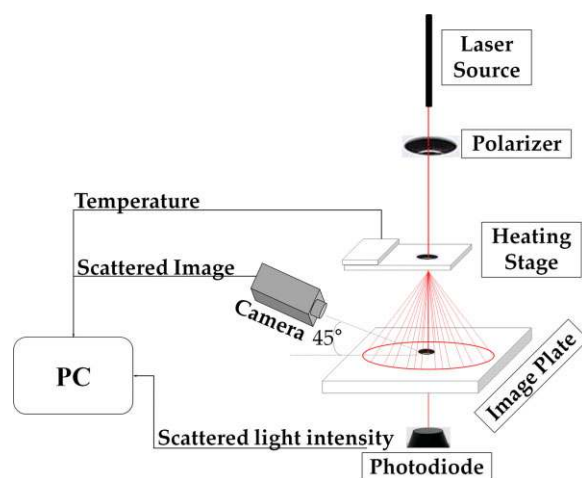


**FIGURE 1** SALS set-up. [Color figure can be viewed in the online issue, which is available at [www.interscience.wiley.com](http://www.interscience.wiley.com).]

fractions of the solvent and the polymer. Then the equation is divided by the overall volume to obtain the Gibbs free energy per unit volume,  $\Delta G_v$ . This can be expressed as a function of intensive parameters as previously discussed elsewhere;<sup>15</sup>

$$\frac{\Delta G_v}{RT} = \left\{ \frac{\phi_1}{V_1} \ln \phi_1 + \frac{\phi_2}{V_2} \ln \phi_2 \right\} + \{ \phi_1 \phi_2 \chi_{12} \} \quad (1)$$

The subscripts 1 and 2 correspond to DMS and epoxy polymer in this case.  $\phi_i$ s are the volume fractions, and  $V_i$ s are the molar volumes of the compounds.  $R$  is the ideal gas constant, and  $T$  is the absolute temperature.  $\chi_{12}$  is the interaction parameter of the two constituents and it can be expressed as a function of the solubility parameters.

In thermoset polymer blends, the Gibbs free energy of mixing is altered by the reaction conversion because of the increase in the molar mass, change in density, and change in the solubility parameter of the curing thermoset. The evolution of the molar volume was discussed previously by Vasquez et al.,<sup>18</sup> and the change in molar volume is formulated with respect to percent conversion by Mezzenga et al.<sup>15</sup>

In the case of small molecules like DMS, and in the case of macromolecules like polymers, the solubility parameters can also be calculated by the Van Krevelen's approach.<sup>19</sup> The solubility parameter of a polymer refers to the repetitive unit of the polymer and it is a function of chain length. Therefore, percent conversion plays an important role in solubility parameter evolution. The evolution of the solubility parameter of a curing thermoset was modeled by Kiefer et al. and it was shown to be increasing almost linearly with conversion.<sup>17</sup> An isophorone diamine cured DGEBA system was investigated in a later study by Mezzenga,<sup>16</sup> where they also observed linear relation, though with a minor deviation ( $\sim 1\%$ ). The tendency is expected to be universal for amine cured epoxies and it is small enough to be neglected. Thus, a linear trend is considered for the calculations in this study

and these calculations are used for the purpose of screening prediction solely.

The reaction conversion is obtained from isothermal DSC experiments. Considering the changes in molar volume, solubility parameter, and molecular weight between crosslinks due to evolution of polymerization reaction, entropic and enthalpic contributions of the FH equation is modified. The Gibbs free energy of mixing diagrams was plotted as a function of conversion to construct the binodal and spinodal curves.

As given in Figure 2, phase separation of DMS is predicted below the gelation point of the curing system for an isothermal curing at 50 °C. It is important to note that the polymer volume fraction in this case is a pseudovolume fraction since polymer is actually evolving (curing) with time.

The aim of this prediction is not to prove or validate the phase separation behavior; indeed, it is conducted for screening. A good deal amount of work needs to be done accounting for more precise assumptions, such as molecular interactions like hydrogen bonding, yet this discussion is out of the scope of this study.

#### Miscibility and Crystallization Behavior

The miscibility of DMS in neat DGEBA monomer (without the crosslinker) was investigated through DSC experiments. The first cooling scans of the DGEBA-DMS mixtures are given in Figure 3. Pure DMS crystals show two distinct crystallization peaks ( $T_c$ ) at 66 and 74 °C in an unusual way by forming a loop. The loops in the exotherm are formed due to the very rapid crystallization and, thus, self-heating of the DMS molecules during cooling, which is a typical response observed in supercooled liquids, usually in metals.<sup>20</sup>

The 25% blend crystallizes at two distinct temperatures at 50 and 71 °C, whereas the 20% blend shows two supercooled crystallization peaks at 37 and 34 °C. The 15% blend presents a very small crystallization exotherm at 4 °C. The packing of DMS molecules into a crystalline order shifts to lower temperatures as the DMS composition is decreased. Thus, it is possible for the DMS molecules in 5 and 10 wt % blends to be arrested in a supercooled liquid or a glassy phase as the DGEBA matrix vitrifies before the DMS molecules can crystallize. The effect of the vitrification of the DGEBA matrix is more pronounced in Figure 4, where the thermal hysteresis between the melting and crystallization curves of the pure DMS and DGEBA-DMS blends are plotted. The thermal hysteresis increases rapidly with decreasing DMS volume fraction. However, at lower concentrations hysteresis is not observed as DMS molecules cannot pack into a crystalline order because of the vitrification of the DGEBA matrix.

The exotherms in pure DMS exhibits similar crystallization enthalpies ( $\Delta H_c$ ) at the onset of crystallization. However, the relative  $\Delta H_c$  in the 25% blend shows a big deviation from 38 to 0.6 J/g between the two exotherms. The 20% blend also gives a similar change in the relative intensity of the enthalpies where the deconvoluted peaks have  $\Delta H_c$  values of

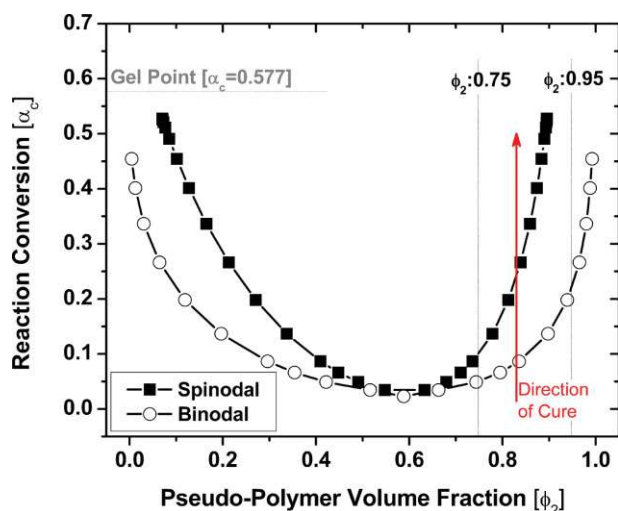


**FIGURE 2** Binodal and spinodal curves of the isothermally cured DMS modified DGEBA-mPDA thermoset. Arrow on the right shows the direction of cure: pointing towards increasing conversion. [Color figure can be viewed in the online issue, which is available at [www.interscience.wiley.com](http://www.interscience.wiley.com).]

13 and 23 J/g. Furthermore, the full width half maximum,  $\Delta w$ , is calculated from crystallization ( $\Delta w_c$ ) peaks.  $\Delta w$  is dependent on the crystal size distribution, the larger the  $\Delta w$  value, the wider the size distribution is.<sup>21</sup> Note the  $\Delta w_c$  values decrease as the DMS composition in the blend increases (see Fig. 5), which implies that the size distribution of DMS crystals get narrower as one puts more DMS into the blends. This further suggests that when the DMS concentration increases, it is easier for DMS molecules to coalesce and form crystals. Therefore, the rate of crystal nucleation is faster, which in turn yields crystals with similar sizes, and narrows the distribution.

Figure 6 illustrates the second heating scan of the blends following the initial cooling scan discussed earlier. The first

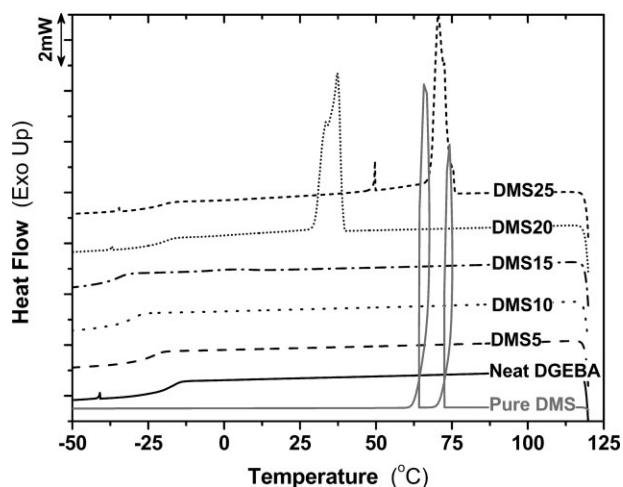


**FIGURE 3** DSC thermograms, obtained from the first cooling scans of the DGEBA-DMS blends are plotted.

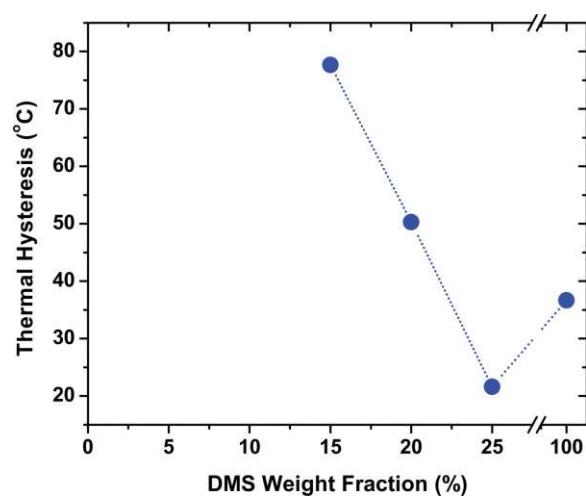


**FIGURE 4** Thermal hysteresis between the melting and crystallization of the DMS molecules are plotted. [Color figure can be viewed in the online issue, which is available at [www.interscience.wiley.com](http://www.interscience.wiley.com).]

point to note is that there is an observed depression in the melting points of the composites. The pure DMS crystals show melting point at 111 °C with a melting enthalpy ( $\Delta H_m$ ) of 207 J/g. The  $\Delta H_m$  of DMS crystals in DGEBA blends decreases to 35.3, 35.2, 24, 14, and 0.40 J/g as the DMS composition decreases from 25 to 5 wt %. The percent crystallinity of DMS in the blends is normalized with respect to the weight fraction of the DMS content and the percent values are calculated by dividing the relative enthalpies to bulk DMS melting enthalpy. Figure 5 suggests that DMS crystallinity increases with increasing DMS concentration. The crystallinity of DMS molecules is very low at lower weight fractions, which suggests that most of the DMS is in its supercooled liquid state or in its glassy state and miscible in the DGEBA matrix. The maximum percent crystallinity is observed for 20% blend where the crystallinity was calculated as 86%. The remaining 14% of the DMS molecules are miscible in the DGEBA matrix. The decrease in DMS crystallinity corresponding to the 25% blend can be attributed to the poor mixing of the blend where the actual DMS content cannot be evaluated reliably.

The correlation between the change in melting point and change in the DMS crystallite size follows the Gibbs-Thomson relation:<sup>22</sup>  $T_m(r)/T_m(\infty) \sim 1 - 1/r$ .  $T_m(\infty)$  is the melting point of the bulk crystal,  $T_m(r)$  is the melting point of the crystal of size  $r$  in a solution, and  $r$  is the crystal size (It is assumed that the DMS retains its bulk properties for  $\Delta H_c$  and density. Expected changes are out of the scope of this work. This relation is only used for a qualitative description.). This relation is in good agreement with experimental data when  $r \geq 10$  nm as discussed by other authors.<sup>22,23</sup> Qualitatively, it suggests that the melting point of the DMS crystals decreases with a reduction in the crystal size. This, in turn, implies that the size of the DMS crystals in the blend decreases with DMS concentration.

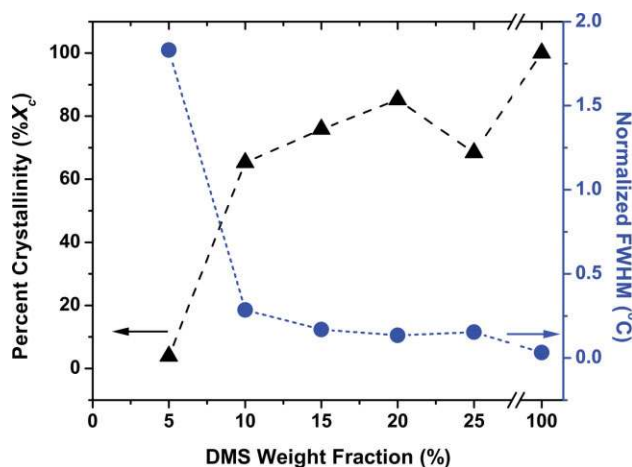


**FIGURE 5** Percent crystallinity of DMS molecules (dashed line with triangles), and FWHM values from DMS crystallization exotherms (dotted line with circles) are plotted. [Color figure can be viewed in the online issue, which is available at [www.interscience.wiley.com](http://www.interscience.wiley.com).]

Deviations in the crystallization behavior, like changes in relative crystallization peaks and relative enthalpies, raise questions about changing the DMS crystal structure. However, X-ray film diffraction studies do not show a significant change in the crystal packing of the DMS molecules (Fig. 7). The data shows neither a change in peak positions nor formation of new peaks at different scattering angles. There is a difference in relative intensities at some scattering angles (16.36 and 20.43  $2\theta$ ), which is still under investigation. These results suggest that DMS crystallinity is not significantly affected and polymorphs are not observed.

Glass transition temperatures ( $T_g$ ) obtained from the heating scans are plotted in Figure 8. They demonstrate a decreasing trend in  $T_g$  with respect to the neat DGEBA  $T_g$ , which suggests miscibility of DMS in the DGEBA matrix as discussed before in crystallinity analysis. The decrease in  $T_g$  in 5–15 wt % blends suggests an increased DMS miscibility. However,  $T_g$  increases at higher DMS loadings as the majority of the DMS molecules phase separate out in the DGEBA matrix and crystallize upon cooling.

Miscibility and crystallization experiments present the possibility to crystallize DMS in DGEBA matrix at different weight fractions. The changes in the crystallization behavior of DMS as a basis for phase separation and isothermal curing experiments is discussed in the following section.

### Phase Separation

Phase separation and crystallization of the DMS was monitored simultaneously using SALS. Figure 9 summarizes representative data obtained by SALS. The scattering profiles suggest that the DMS molecules phase separate and crystallize under isothermal conditions below 80 °C, which agrees with the DSC results. The profiles further illustrate the time for initial crystal formation and it is observed to increase with the isothermal curing temperature. This suggests that

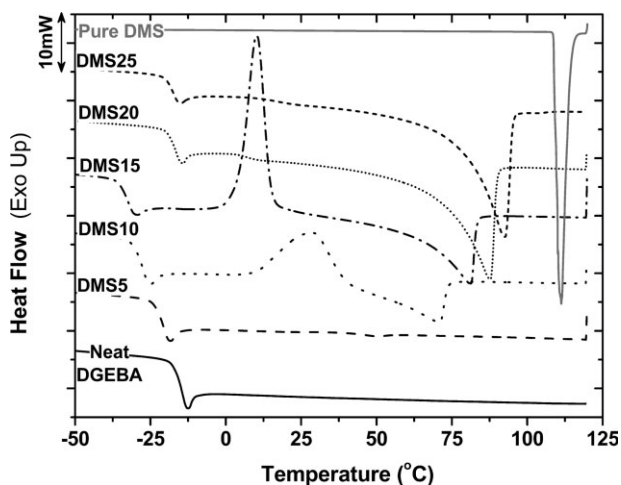


**FIGURE 6** DSC thermograms, obtained from the second heating scans of the DGEBA-DMS blends are plotted.

the degree of supercooling plays a significant role in crystallization kinetics.

The 20 and 25 wt % blends show crystallization of DMS by measuring a significant decrease in scattering intensity. Moreover, the scattering patterns obtained from SALS point out a preferred orientation of the DMS crystals. Although the angle between the predominant directions deviates with temperature, there is still a favored orientation with a bimodal distribution. This directionality results from the faceted crystal front surface morphology as shown in Figure 10.

Optical studies show that the crystal front face is not perpendicular to the radial growth direction. Rather, it forms at a preferred angle that ultimately dictates growth in specific directions. The faceted growth of organic crystals is a well known phenomenon and it is described by part of the surface energy theory,<sup>24</sup> which states that crystal plane with low surface energy grows faster than the crystal plane with a higher surface energy. The variant growth habit in Figure 10b is further triggered by the competition between the

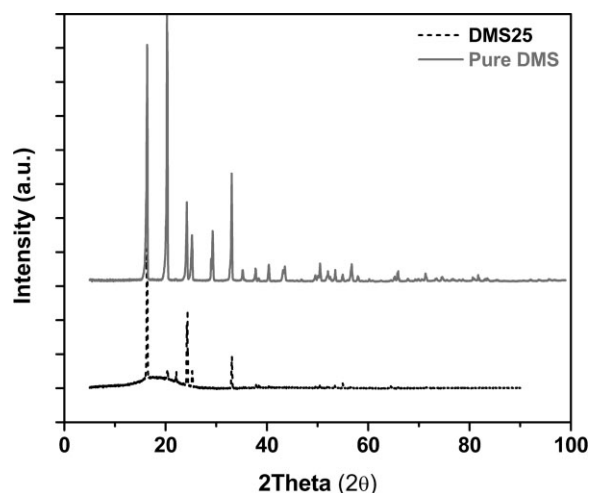


**FIGURE 7** XRD measurements of pure DMS and DMS25 blend.

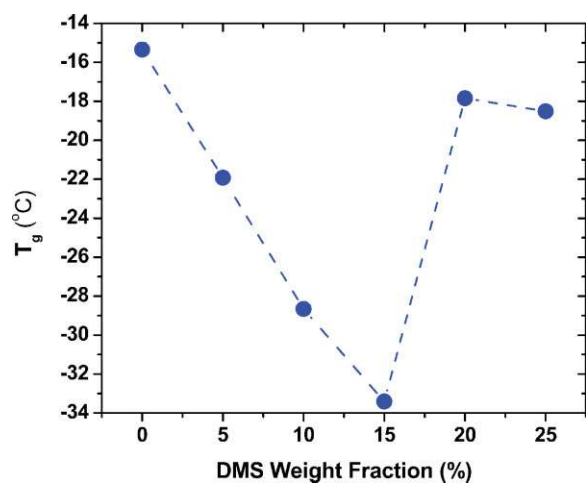


**FIGURE 8** Glass transition temperatures of DGEBA-DMS blends are plotted. [Color figure can be viewed in the online issue, which is available at [www.interscience.wiley.com](http://www.interscience.wiley.com).]

crystallization behavior and different thermal cure conditions. At the end, the competition leads to producing the rich, distinct morphologies. Additionally, Figure 11 shows that the DMS crystals do not disperse easily at low temperatures as they do at higher isothermal conditions. This suggests that the viscosity is significantly affecting the crystallization kinetics and it is high enough to decrease the mobility of the growing DMS crystals at low temperatures.

### Reinforcement Morphologies

One type of morphology observed in this system is the discrete chopped fiber-reinforced morphology, which is illustrated for the case of 15% DMS loaded epoxy in Figure 12. These samples were prepared in 20 mL glass vials following the same procedure given in the experimental section. Figure 12a shows the formation of reinforcements with high volume fractions. Crystals with tens of microns widths are generated with an aspect ratio of  $\sim 40$ . These high aspect ratio crystallites are randomly oriented inside the epoxy matrix by effec-

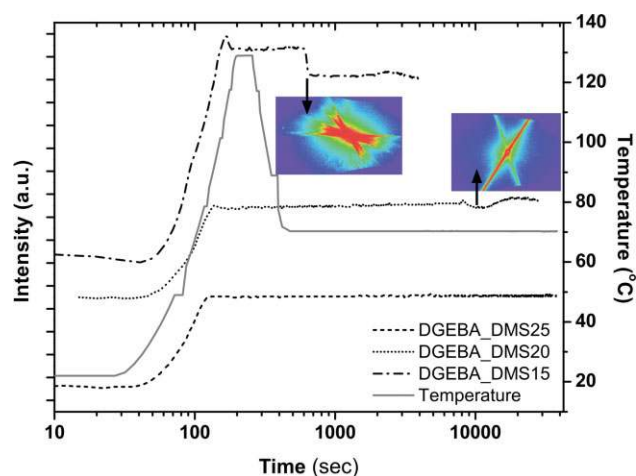


**FIGURE 9** Scattering intensity and time data, obtained from a SALS experiment are given (plotted data is from an isothermal cure conducted at 70 °C). [Color figure can be viewed in the online issue, which is available at [www.interscience.wiley.com](http://www.interscience.wiley.com).]

tively forming isotropic structures. Figure 12b shows that the fiber-like crystals are actually forming bundles of DMS crystallites, which grow adjacent to each other in the same direction. The self-alignment of the locally anisotropic fibers is a part of the phase separation and crystallization processes and observed without any external force fields.

Composites with 15 wt % DMS were prepared at different temperatures. The results impart a broad range of morphologies under certain conditions. Figure 13 shows a selective map of morphologies including the formation of nanoscale wires growing into dendritic type micron-scale crystallites as well as large fiber-like crystals and particles with a wide range of sizes.

Note that the DMS crystals extend to hundreds of microns in length when the conditions are suitably met. At higher initial cure temperatures, the question about the interplay between

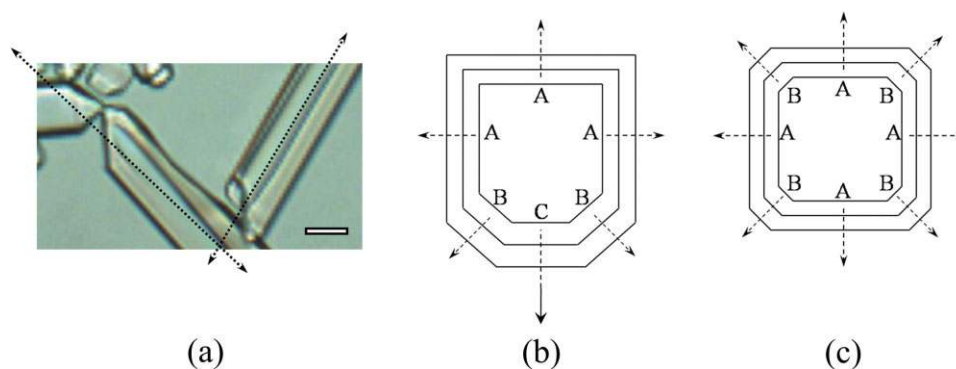


**FIGURE 10** Faceted growth of crystals. (a) Optical micrograph of DMS crystals with faceted crystal front faces. (b) Schematic of a crystal growth in a direction normal to the crystal plane with the lowest surface free energy (C-plane). (c) Schematic of a crystal growth equally in all directions due to crystal planes all having the same surface free energies.<sup>24</sup> [Color figure can be viewed in the online issue, which is available at [www.interscience.wiley.com](http://www.interscience.wiley.com).]

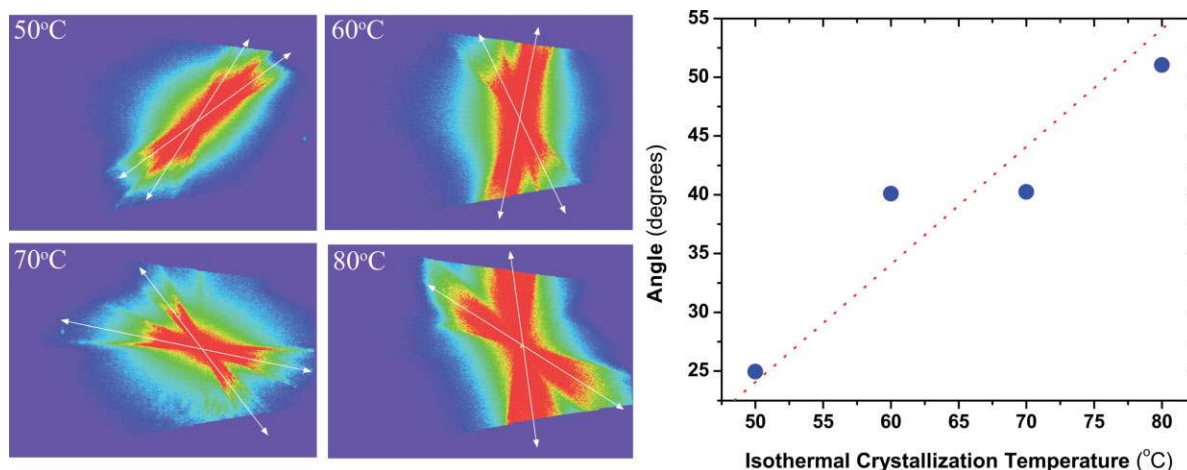


**FIGURE 11** SALS images that were obtained at different isothermal conditions. Angles between the two average predominant directions as a function of temperature are plotted on the right.

the curing epoxy matrix and the crystallization and growth of DMS molecules results in beautiful dendritic morphologies.

Specimens collected from three different temperature regions were characterized by DSC. Figure 14 shows that, the crystal morphologies can be embedded into the thermoset resin depending on the initial curing/crystallization temperatures. Even though the melting point of pure DMS crystals is 111 °C, they are apparently stable at elevated temperatures up to 200 °C. A strong melting endotherm is only observed for the sample that is initially cured at room temperature. This result is still under investigation, but it suggests that the thermal stability of the embedded crystals can be increased when the epoxy matrix is initially cured at higher temperatures. This experiment suggests a potential persistence of the local anisotropy of fiber-like crystals in the epoxy matrix at high temperatures, without the need to use specific chemistries like in LC thermosets.

The images in Figure 15 were obtained by an optical microscope from the samples in the SALS experiments that are

described in the phase separation section. The figure presents a wider expansive map of crystals that can be generated *in situ* at various temperature and concentration levels. Competition between curing and crystallization processes results in various crystallite morphologies and sizes ranging from nanowires to microfibers. It is possible to produce these fruitful morphologies only by adjusting the curing temperature and DMS concentration.

This dendritic morphology is subject of future investigation as it may exhibit different load transfer characteristics. It is also possible to form particles of 200–500 nm scale with higher temperature curing but the concentration and distributions of these crystals are not uniform. On the other hand, at higher DMS concentrations the system generates fiber-like crystals. These discrete fibers grow adjacent to each other to a width of 50  $\mu\text{m}$  and length of couple of centimeters as also discussed in Figures 12 and 13. This type of morphology is very promising in terms of creating long microchannels and distinct reinforcement characteristics as the aspect ratio of these *in situ* generated crystals is greater than 25. Figure 13

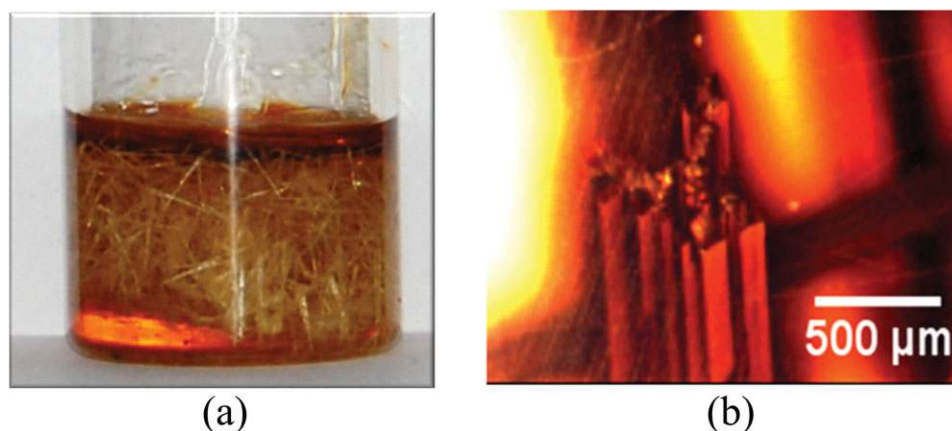


**FIGURE 12** (a) Image of an epoxy specimen loaded with 15% DMS. (b) Image of DMS crystal bundles from the DMS15 specimen given in (a).

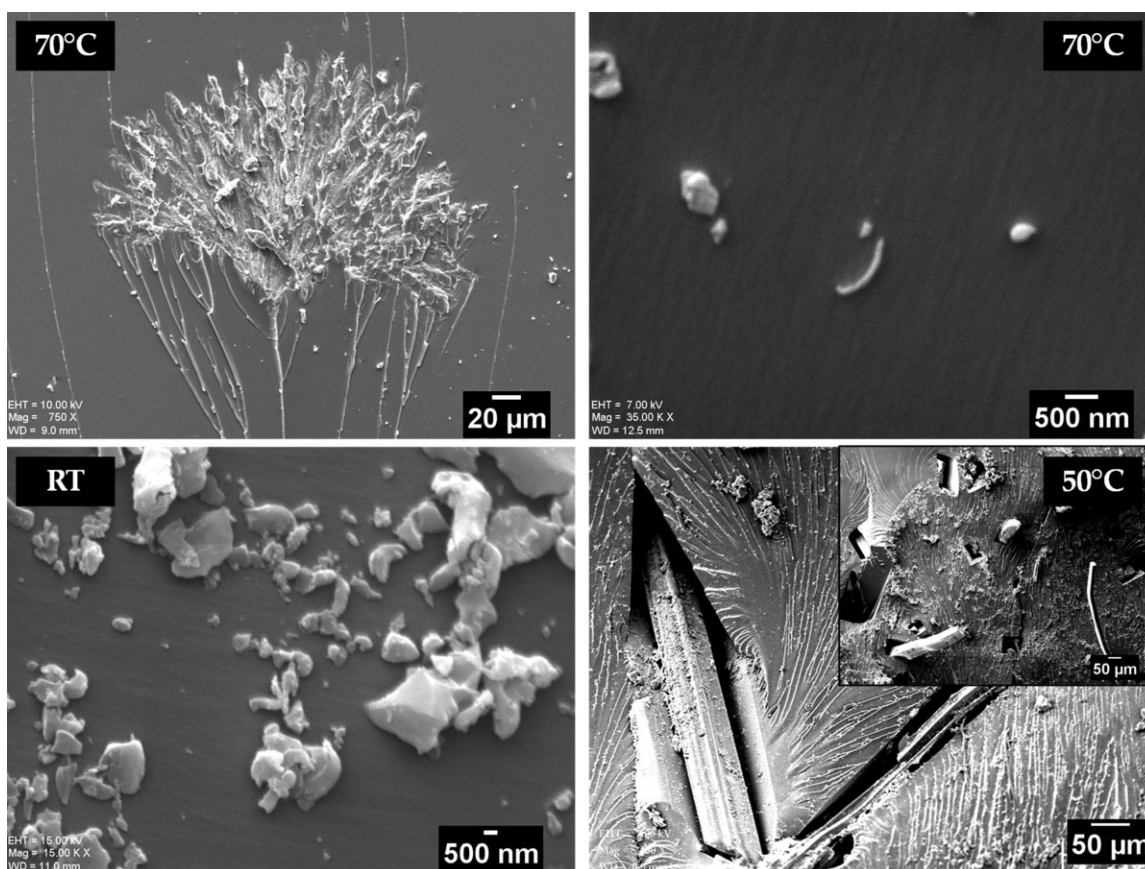


**FIGURE 13** SEM images of DMS15 blend at different cure conditions.

also suggests that as one goes further down the temperature scale, where the system is initially cured at room temperature, then particles with a wide range of crystal sizes are observed. As the DMS molecules are entrapped in the high viscosity resin at low temperatures, the whiskers can still be grown but the large aspect ratio is lost to a great extent.

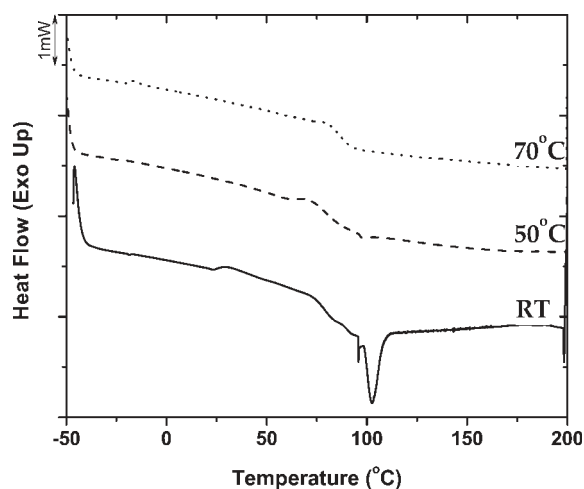


**FIGURE 14** DSC thermograms of DMS15 blends that were initially cured at different temperatures. Samples are fully post-cured at 130 °C.

Instead, nano- to micron-scale particles are mostly formed and the whiskers are much shorter and thinner. The size distribution of these crystals is not optimized yet, but this study emphasizes the great potential to generate distinct, rich morphologies via this approach.

Contrary to LC thermosets, the anisotropy of our *in situ* generated crystals is formed without applying any external force fields. In our case, the anisotropy is a pure effect of the crystallization behavior of DMS molecule. In addition to the broad range of crystal morphologies, the aspect ratio of these *in situ* generated potential reinforcements is remarkably high. Depending on the isothermal conditions, the aspect ratio of the crystal fibers can be more than 100.

## CONCLUSIONS

LMW organic crystal DMS was investigated as potential *in situ* reinforcement in an epoxy thermoset polymeric system. The rate of DMS crystal nucleation and percent crystallinity is found to increase with increasing DMS concentration. SALS profiles obtained after phase separation of DMS during epoxy curing showed faceted growth mechanisms of organic crystals, which lead to the formation of locally anisotropic but spatially isotropic crystal reinforcements. This suggests that the effect of isothermal curing temperature not only affects the mobility of the crystals; thus, level of anisotropy,



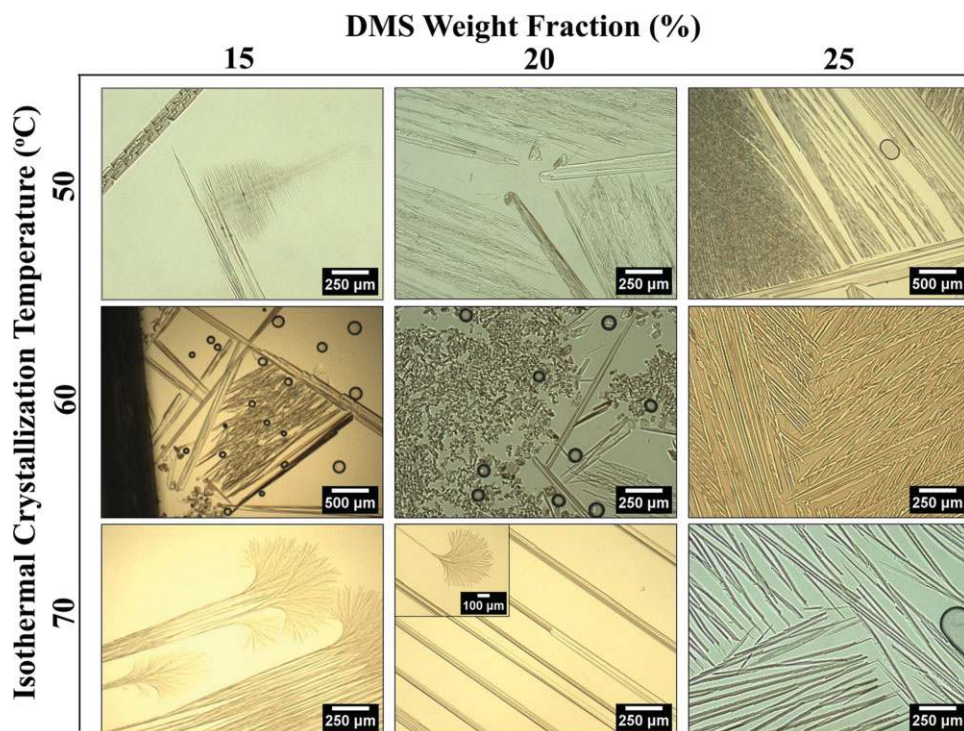


**FIGURE 15** Map of DMS crystal growth habits as a function of concentration and curing temperature is given. [Color figure can be viewed in the online issue, which is available at [www.interscience.wiley.com](http://www.interscience.wiley.com).]

but also affects the agility of individual molecules forming the crystals with different growth habits, such as dendritic and needle-like crystals.

Blends with 15 wt % DMS revealed that the crystals grow in bundles, forming a chopped fiber-like composite structure. The investigation of the effect of temperature in the 15% DMS blends revealed that the anisotropic reinforcements are formed in quiescent conditions and further hybrid morphologies are generated as polymerization reaction continues. We were able to present the formation of nanoscale particles as well as centimeter long fiber-like crystals by adjusting the cure conditions. Changing the cure temperature and LMW compound additive illustrate even a wider map of morphologies, which shows extremely high aspect ratio crystals and distinct hybrid morphologies. The interplay between the crosslinking reaction and the crystallization of DMS generates these morphologies and they can be changed from compound to compound.

This study demonstrated an alternate approach to reinforce thermosets *in situ*, by using LMW crystallizable solvents. LMW additives generate very rich morphologies of reinforcements via the competition between the curing reaction of the thermoset and the phase separation-crystallization of the additive. The authors believe that the broad range of morphologies generated *in situ* by this approach is propitious in a wide variety of engineering applications, such as electronics, microfluidics, and novel anchoring mechanisms of the discrete fibers to the matrix to improve mechanical properties.

## REFERENCES AND NOTES

- Kalapasrad, G.; Mathew, G.; Pavithran, C.; Thomas, S. *J Appl Polym Sci* 2003, 89, 432–442.
- Joshi, M.; Maiti, S. N.; Misra, A. *Polymer* 1994, 35, 3679–3685.
- Hassan, A.; Yahya, R.; Yahaya, A. H.; Tahir, A. R. M.; Hornsby, P. R. *J Reinforced Plastics Compos* 2004, 23, 969–986.
- Joseph, P. V.; Mathew, G.; Joseph, K.; Thomas, S.; Pradeep, P. *J Appl Polym Sci* 2003, 88, 602–611.
- Ozkoc, G.; Bayram, G.; Bayramli, E. *Polym Compos* 2005, 26, 745–755.
- Ortiz, C.; Kim, R.; Rodighiero, E.; Ober, C. K.; Kramer, E. J. *Macromolecules* 1998, 31, 4074–4088.
- Carfagna, C.; Amendola, E.; Giamberini, M. *Prog Polym Sci* 1997, 22, 1607–1647.
- Barclay, G. G.; McNamee, S. G.; Ober, C. K.; Papatomas, K. I.; Wang, D. W. *J Polym Sci Part A: Polym Chem* 1992, 30, 1845–1853.
- Lesser, A. J.; Calzia, K.; Junk, M. *Polym Eng Sci* 2007, 47, 1569–1575.
- Yoon, J.; McCarthy, T. J.; Lesser, A. J. *J Appl Polym Sci* 2009, 113, 3564–3576.
- Lesser, A. J.; McCarthy, T. J.; Yoon, J.; Yordem, O. S. *Reinforced Polymeric Materials, Methods of Manufacture Thereof and Articles Comprising the Same*. University of Massachusetts, Amherst, WO/2008/121798, September 10, 2008.

- 12** Oyanguren, P. A.; Frontini, P. M.; Williams, R. J. J.; Vigier, G.; Pascault, J. P. *Polymer* 1996, 37, 3087–3092.
- 13** Narkis, M.; Siegmann, A.; Puterman, M.; Di Benedetto, A. T. *J Polym Sci: Polym Phys Ed* 1979, 17, 225–234.
- 14** Flory, P. J. *Principles of Polymer Chemistry*; Cornell University Press: Ithaca, NY, 1967.
- 15** Mezzenga, R.; Boogh, L.; Månson, J.-A. E. *J Polym Sci Part B: Polym Phys* 2000, 38, 1893–1902.
- 16** Mezzenga, R.; Boogh, L.; Månson, J.-A. E. *J Polym Sci Part B: Polym Phys* 2000, 38, 1883–1892.
- 17** Kiefer, J.; Hilborn, J. G.; Hedrick, J. L. *Polymer* 1996, 37, 5715–5725.
- 18** Vasquez, A.; Rojas, A. J.; Adabbo, H. E.; Borrajo, J.; Williams, J. J. *Polymer* 1987, 28, 1156–1164.
- 19** Van Krevelen, D. W. *Properties of Polymers: Their Correlation with Chemical Structure, Their Numerical Estimation and Prediction from Additive Group Contributions*; Elsevier: Amsterdam, New York, 1990.
- 20** Anestiev, L.; Malakhov, D. *J Noncrystalline Solids* 2006, 352, 3350–3355.
- 21** Gupta, A. K.; Rana, S. K.; Deopura, B. L. *J Appl Polym Sci* 1992, 44, 719–726.
- 22** Jackson, C. L.; McKenna, G. B. *J Chem Phys* 1990, 93, 9002–9011.
- 23** Jiang, Q.; Shi, H. X.; Zhao, M. *J Chem Phys* 1999, 111, 2176–2180.
- 24** Mullin, J. W. *Crystallization*; Butterworth-Heinemann: Oxford, 2001.